Implementation schemes for unsharp measurements with trapped ions

Sujit K. Choudhary,[1,*] T. Konrad,[1,2,†] and H. Uys[3,‡]

[1]*School of Chemistry and Physics, University of KwaZulu-Natal, Durban 4001, South Africa*

[2]*National Institute of Theoretical Physics, University of KwaZulu-Natal, Durban 4001, South Africa*

[3]*National Laser Centre, Council for Scientific and Industrial Research, Pretoria 0001, South Africa*

(Received 9 November 2012; published 31 January 2013)

Unsharp positive operator-valued measurements allow a variety of measurement applications which minimally disrupt the state of the quantum system. Experimental schemes are proposed for implementing unsharp measurements on the qubit levels of a trapped ion. The schemes rely on introducing weak entanglement between the state of a target ion and that of an auxiliary ion, using standard ion-trap quantum logic operations, and then realizing an unsharp measurement through projective measurement on the auxiliary atom. We analyze common sources of error and their effect on different applications of unsharp measurements.

DOI: 10.1103/PhysRevA.87.012131 PACS number(s): 03.65.Ta, 37.10.Ty, 42.50.−p

I. INTRODUCTION

Recent years have witnessed considerable interest in the experimental and theoretical study of single quantum systems in atomic traps, optical cavities, and coupled quantum dots. In trapped-ion physics experiments a comprehensive toolbox of control techniques has been developed, allowing implementation of all single- and two-qubit quantum gates required for quantum computing [1]. This quantum control toolbox has enabled new methods of precision measurement [2], fundamental studies [3], and quantum simulation [4]. A tool set which hitherto has not been fully explored experimentally is that of generalized, positive operator-valued measure (POVM) measurements [5]. The POVM formalism describes all measurements allowable within the limits of quantum theory. Such measurements may be implemented by performing a unitary interaction between a target system and an auxiliary system, and then performing a projective measurement on the auxiliary system. One advantage of POVM measurements is that they can be made "unsharply" (weakly), so that any individual unsharp measurement does not project the quantum state into an eigenstate of the measured observable and thus does not strongly disrupt the state dynamics.

The quantum-state evolution resulting from unsharp measurement has been experimentally studied in superconducting qubits [6]. The utility of unsharp measurements has also been demonstrated experimentally in, for example, the quantum feedback stabilization of photon number in a microwave cavity [7], and in the improved state preparation of a photon wave function through quantum feedback after an unsharp measurement [8]. We showed earlier [9] that it is possible, in principle, to monitor (approximately) the dynamics (Rabi oscillations) of a single two-level quantum system in real time using unsharp measurements, or to estimate the Rabi frequency [10,11], while only weakly influencing the original dynamics. By using unsharp measurement estimation in conjunction with feedback, Vijay *et al.* recently demonstrated stabilization of Rabi oscillations in a superconducting qubit at a desired frequency [12–14]. Furthermore, it has been shown experimentally that the partial collapse due to weak measurements on photonic qubits can be (probabilistically) reversed [15], and the theory of such reversal has been investigated for solid-state qubits [16]. Finally, an experimental setup for visualizing a photon oscillating between two cavities has also been proposed [17].

This article demonstrates how to implement a class of symmetric POVM measurements on the hyperfine qubit levels of trapped ions, thus expanding the set of quantum measurement tools in this field. We exploit standard techniques of trapped-ion quantum control to achieve this goal. The rest of this article is structured as follows. In Sec. II we provide some theoretical background on POVM measurement, while in Sec. III we present two schemes for implementing unsharp measurements. The efficiency of individual measurements is then analyzed in the light of various experimental imperfections in Sec. IV. Finally, in Sec. V we discuss two examples of applications of unsharp POVM measurements and the consequences of experimental imperfections for these applications.

II. POVM FORMALISM

Usual quantum measurements project the initial state of a system onto one of the eigenstates of the observables being measured. For example, in a measurement of spin along direction $\hat{r}$, the projectors onto the eigenstates are

$$\hat{P}_{\pm} = \tfrac{1}{2}[\mathbb{I} \pm \hat{r}\cdot\vec{\sigma}], \tag{1}$$

where $\mathbb{I}$ denotes the identity operator and $\vec{\sigma} = (\hat{\sigma_x},\hat{\sigma_y},\hat{\sigma_z})$ is the usual Pauli operator. Projective measurements only represent a restricted set of allowed measurements within quantum theory. In the more general framework, the states of a quantum system are represented by positive trace class operators. Any observable is represented by a collection of positive operators $\{E_i\}$ where $\sum_i E_i = \mathbb{I}$, and every eigenvalue λ of each operator E_i obeys the bound $0 \leqslant \lambda \leqslant 1$. In a measurement of such an observable for the state ρ (say), the probability of occurrence of the ith result is given by $\mathrm{Tr}[\rho E_i]$. Unlike projective measurement, knowing the operators $\{E_i\}$ is, in general, not enough to determine the state of the system after measurement; we further need to know the operators $\hat{M}_i$ constituting the POVM elements $\{E_i\}$. As an example, let

*choudhary@ukzn.ac.za
†konradt@ukzn.ac.za
‡huys@csir.co.za

$E_i = \sum_j M_{ij}^\dagger M_{ij}$, then after the outcome i is detected, the state is $\rho \mapsto \rho' = \frac{1}{\mathrm{Tr}[\rho E_i]} \sum_j M_{ij} \rho M_{ij}^\dagger$. This measurement does not in general preserve the purity of states unless there is a single M_{ij} for each E_i. In that case the postmeasured state is given by

$$|\psi'\rangle = \frac{M_i|\psi\rangle}{\sqrt{\langle\psi|M_i^\dagger M_i|\psi\rangle}}. \tag{2}$$

We concern ourselves only with the set of symmetric measurement operators

$$\hat{M}_0 = \sqrt{p_0}\ \hat{P}_+ + \sqrt{1-p_0}\ \hat{P}_-, \tag{3}$$

$$\hat{M}_1 = \sqrt{1-p_0}\ \hat{P}_+ + \sqrt{p_0}\ \hat{P}_-, \tag{4}$$

related via

$$M_0^\dagger M_0 + M_1^\dagger M_1 = \mathbb{I}, \tag{5}$$

and $0 \leqslant p_0 \leqslant 0.5$. The positive operators $M_i^\dagger M_i$ $(i \in 0,1)$ constitute the POVM elements and are interpreted as dichotomic observables (for example, spin observable of a spin-1/2 particle, energy of a two-level system, etc.). The measurement strength (sharpness) is parametrized by the quantity $\Delta p = (1-p_0) - p_0 = 1 - 2p_0$. For $\Delta p = 1$, it represents the usual projective (sharp) measurement, while $\Delta p = 0$ represents an infinitely weak (unsharp) measurement, which yields no information and does not change the state of the system.

III. IMPLEMENTATION SCHEMES

We now show that trapped ions provide a realistic system to implement the generalized measurement given by Eqs. (3) and (4). As an example we choose $\hat{P}_\pm = (\mathbb{I} \pm \hat{\sigma}_z)/2$, but we show in the Appendix how to generalize this for arbitrary projectors, Eq. (1). Two schemes are described, both relying on standard techniques used in ion-trap quantum control experiments to generate entanglement.

A. Scheme I

In the first scheme we consider two ions, of different species, to be trapped in the same ion trap, thus sharing collective vibrational (phonon) modes. One ion is the target system, of which we wish to measure some observable unsharply. We label its internal state with the ket $|\psi_t\rangle$. The second is an auxiliary ion, described by $|\psi_a\rangle$, which is used both for sympathetic cooling of the phonon modes and for assisting in implementing the unsharp measurement. Since the ions are of different species, any light field used to manipulate one ion does not affect the other ion, obviating the need for addressing ions independently.

Both ion species need to be carefully chosen to have appropriate level structures to enable the measurement scheme. For the target ion we choose two hyperfine (qubit) ground levels $|g_t\rangle$ and $|e_t\rangle$ and aim to measure the z component of its effective spin, $\hat{\sigma}_z$, unsharply. This is accomplished with the assistance of a third metastable excited state, $|r_t\rangle$, as shown in Fig. 1 (or a stimulated Raman transition to a third hyperfine ground state). A metastable state is chosen so as to minimize the effects of spontaneous emission. Figure 1 further indicates

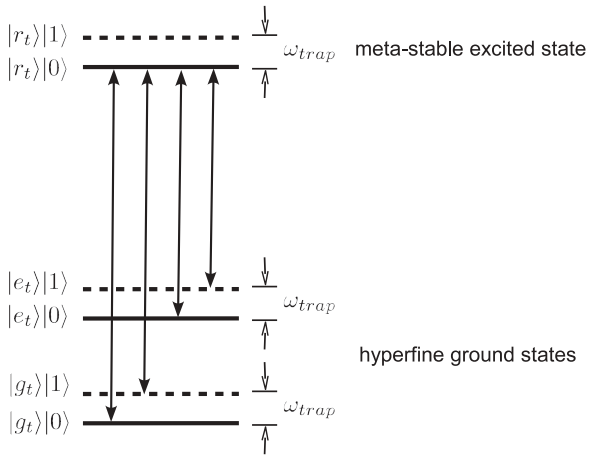

FIG. 1. Unsharp measurement of a spin component of a two-level transition $|g_t\rangle \longrightarrow |e_t\rangle$ requires an auxiliary metastable level $|r_t\rangle$ (scheme I). In the Lamb-Dicke regime the energy spectrum of the ion exhibits resonance not only at the carrier laser frequency but also at the sidebands detuned by a vibrational frequency ω_{trap}. The number of excitations of the vibrational mode is indicated by the right-hand ket.

that the ion's energy spectrum incorporates excitations of the vibrational modes; i.e., $|g_t\rangle|0\rangle$ describes the state where the ion is in the electronic ground state, $|g_t\rangle$, and the vibrational state, $|0\rangle$, of the ion has zero phonons (vibrational ground state). The internal structure of the auxiliary atom must allow quantum logic spectroscopy (QLS) [2] measurements, which are discussed later.

Given that the target ion is in the desired state to be measured unsharply, the measurement scheme can be divided into four stages:

(1) Sympathetic cooling to the vibrational ground-state on the auxiliary ion,

(2) Repump state preparation of the auxiliary atom,

(3) Unitary unsharp measurement preparation of both ions, and

(4) Unsharp measurement execution through QLS on the auxiliary ion.

Moreover, the system is assumed to be in the Lamb-Dicke regime [18] so that the vibrational sidebands of the internal transitions are resolved. This implies that a light field detuned to the red (blue) of a ground-to-excited-state transition by a motional mode frequency ω_{trap} will lead to the absorption (emission) of a vibrational phonon, and vice versa.

If initially the target atom is prepared in a coherent superposition of its qubit levels $|\psi_t^{(0)}\rangle = c_1|g_t\rangle + c_2|e_t\rangle$, then, after the ground-state cooling stage on the auxiliary ion, the state of the system can be described by

$$|\psi\rangle = |\psi_t^{(0)}\rangle|\psi_a\rangle|0\rangle \tag{6a}$$

$$= (c_1|g_t\rangle + c_2|e_t\rangle)|\psi_a\rangle|0\rangle, \tag{6b}$$

where $|c_1|^2 + |c_2|^2 = 1$. The measurement preparation stage consists of a sequence of four laser pulses applied to the target atom (as illustrated in Fig. 2):

(1) A pulse on resonance with the transition $|g_t\rangle \longrightarrow |r_t\rangle$ (carrier pulse) for a duration $t = (2/\Omega_1)\cos^{-1}(\sqrt{p_0})$ [Fig. 2(a)], (Ω_1 is the Rabi frequency connecting $|g_t\rangle$ and

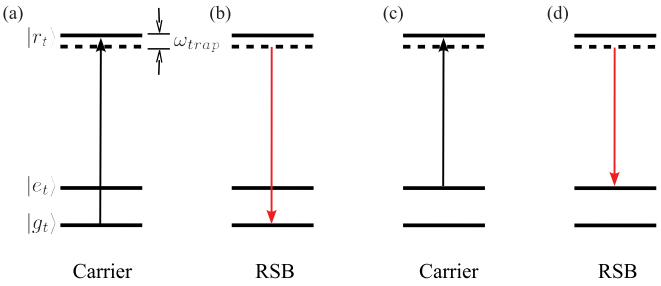

FIG. 2. (Color online) Sequence of laser pulses on an ion to prepare it to the desired state, Eq. (10), for unsharp measurement of $\hat{\sigma}_z$ through scheme I.

$|r_t\rangle$), leading to the state

$$|\psi_1\rangle = [c_1(\sqrt{p_0}|g_t\rangle + \sqrt{1-p_0}|r_t\rangle) + c_2|e_t\rangle]|\psi_a\rangle|0\rangle. \quad (7)$$

(2) A pulse on the same transition, but red-detuned by a motional mode frequency [red sideband (RSB) pulse] [Fig. 2(b)], causing the transition $|r_t\rangle|0\rangle \longrightarrow |g_t\rangle|1\rangle$. The component $|g_t\rangle|0\rangle$ of $|\psi_1\rangle$ remains unaffected by this pulse as the state $|r_t\rangle|-1\rangle$ does not exist [1,18]. This results in the following two-ion state:

$$|\psi_2\rangle = [c_1|g_t\rangle(\sqrt{p_0}|0\rangle + \sqrt{1-p_0}|1\rangle) + c_2|e_t\rangle|0\rangle]|\psi_a\rangle. \quad (8)$$

(3) A carrier pulse on resonance with the transition $|e_t\rangle \longrightarrow |r_t\rangle$ of duration $t = (2/\Omega_2)\cos^{-1}(\sqrt{1-p_0})$ (where Ω_2 is the Rabi frequency connecting $|e_t\rangle$ and $|r_t\rangle$), [Fig. 2(c)]. This transforms the state to

$$\begin{aligned}|\psi_3\rangle = [&c_1|g_t\rangle(\sqrt{p_0}|0\rangle + \sqrt{1-p_0}|1\rangle) \\ &+ c_2(\sqrt{1-p_0}|e_t\rangle + \sqrt{p_0}|r_t\rangle)|0\rangle]|\psi_a\rangle. \end{aligned} \quad (9)$$

(4) Finally, a red sideband pulse between $|e_t\rangle$ and $|r_t\rangle$ [Fig. 2(d)] yielding

$$\begin{aligned}|\psi_4\rangle &= [c_1|g_t\rangle(\sqrt{p_0}|0\rangle + \sqrt{1-p_0}|1\rangle) \\ &\quad + c_2|e_t\rangle(\sqrt{1-p_0}|0\rangle + \sqrt{p_0}|1\rangle)]|\psi_a\rangle \\ &= [(\sqrt{p_0}c_1|g_t\rangle + \sqrt{1-p_0}c_2|e_t\rangle)|0\rangle \\ &\quad + (\sqrt{1-p_0}c_1|g_t\rangle + \sqrt{p_0}c_2|e_t\rangle)|1\rangle]|\psi_a\rangle. \end{aligned} \quad (10)$$

The generalized measurements of Eqs. (3) and (4) on the internal degrees of freedom of the target ion can now be realized by performing a projective measurement on the vibrational state, because measuring in the $\{|0\rangle,|1\rangle\}$ basis projects the internal state of the target ion onto either of the two states

$$(\sqrt{p_0}c_1|g_t\rangle + \sqrt{1-p_0}c_2|e_t\rangle)$$

or

$$(\sqrt{1-p_0}c_1|g_t\rangle + \sqrt{p_0}c_2|e_t\rangle).$$

This sequence is equivalent to applying the measurement operators $\hat{M}_0$ or $\hat{M}_1$ to the initial state of the target atom:

$$\hat{M}_0|\psi_t^{(0)}\rangle; \hat{M}_0 = \sqrt{p_0}|g_t\rangle\langle g_t| + \sqrt{1-p_0}|e_t\rangle\langle e_t|, \quad (11)$$

and

$$\hat{M}_1|\psi_t^{(0)}\rangle; \hat{M}_1 = \sqrt{1-p_0}|g_t\rangle\langle g_t| + \sqrt{p_0}|e_t\rangle\langle e_t|. \quad (12)$$

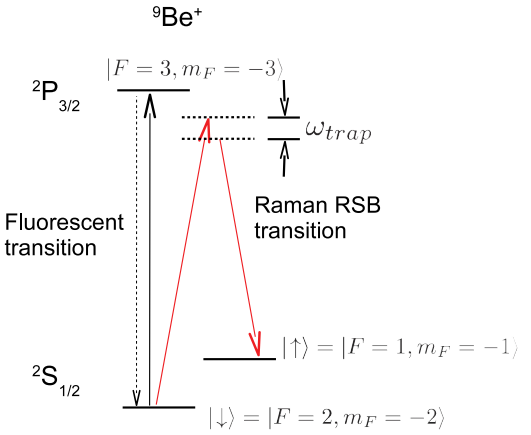

FIG. 3. (Color online) $^9Be^+$ energy levels used for quantum logic spectroscopy detection of the motional state of the two-ion system. A Raman red sideband pulse, red (grey) lines, transfers the auxiliary ion to a dark state, $|^2S_{\frac{1}{2}}, F=1, m_F=-1\rangle$, only if a vibrational excitation is present. Subsequent fluorescence (or not) on the $|^2S_{\frac{1}{2}}, F=2, m_F=2\rangle \longrightarrow |^2P_{\frac{3}{2}}, F=3, m_F=3\rangle$ transition projects the vibrational state onto $|0\rangle(|1\rangle)$ [2].

Projection onto the vibrational state is accomplished through a QLS measurement [2], which we briefly review. QLS maps the vibrational state of the two-ion system onto a dark (bright) hyperfine, ground-state level of the auxiliary ion, conditioned on the presence (or absence) of a vibrational excitation. A subsequent fluorescence detection measurement of the auxiliary ion state completes the measurement. Let us denote the qubit levels of the auxiliary ion with $|\downarrow\rangle,|\uparrow\rangle$. The required level structure for the auxiliary ion is shown in Fig. 3. $^9Be^+$ is a suitable candidate if we associate $|\downarrow\rangle \equiv |^2S_{\frac{1}{2}}, F=2, m_F=-2\rangle$ and $|\uparrow\rangle \equiv |^2S_{\frac{1}{2}}, F=1, m_F=-1\rangle$. We assume that the internal state of the auxiliary ion was initially prepared in level $|\downarrow\rangle$, so that after the measurement preparation sequence the full state of the system is

$$\begin{aligned}|\Psi\rangle = &[\sqrt{p_0}c_1|g_t\rangle + \sqrt{1-p_0}c_2|e_t\rangle]|0\rangle|\downarrow\rangle \\ &+ [\sqrt{1-p_0}c_1|g_t\rangle + \sqrt{p_0}c_2|e_t\rangle]|1\rangle|\downarrow\rangle. \end{aligned} \quad (13)$$

A Raman red sideband pulse on the auxiliary ion, illustrated in Fig. 3, transfers the final state of the two-ion system to

$$\begin{aligned}|\Psi_f\rangle = &[(\sqrt{p_0}c_1|g_t\rangle + \sqrt{1-p_0}c_2|e_t\rangle)|\downarrow\rangle \\ &+ (\sqrt{1-p_0}c_1|g_t\rangle + \sqrt{p_0}c_2|e_t\rangle)|\uparrow\rangle]|0\rangle. \end{aligned} \quad (14)$$

Because $|\downarrow\rangle$ fluoresces strongly, whereas $|\uparrow\rangle$ is dark to the detection light [2], we can measure the final state of the auxiliary ion sharply, thereby executing the unsharp measurement, Eqs. (11) and (12), on the target ion.

B. Scheme II

Scheme I, discussed above, has the advantage that two different ion species are used, making the target qubit states immune to spontaneous emission from laser light addressing the auxiliary ion. We now discuss a different scheme using two ions of the same species, but with a simpler pulse sequence. The scheme is based on the Kitegawa squeezing Hamiltonian

[19]:

$$H_S = \hbar \frac{\chi}{2} J_z^2, \tag{15}$$

where $\hat{J}_z = \sum_j \hat{\sigma}_j^z$ is the collective spin operator. This Hamiltonian is routinely used to implement geometric phase gates in quantum information processing experiments, by exerting a spin-state-dependent optical dipole force on the ions using far off-resonant laser beams [20]. Since the experimental approach is well known, we simply discuss how it enables unsharp measurement.

We again consider two ions, target and auxiliary, in the same trap. The ions have suitable qubit levels and excited states allowing repumping, cooling, and fluorescence detection. The scheme consists of four stages:

(1) Cooling of the auxiliary ion, thus cooling the target ion sympathetically,
(2) State preparation (repump) of the auxiliary ion,
(3) Unsharp measurement preparation on both ions, and
(4) Fluorescence detection of the auxiliary ion state.

Since both ions are of the same species, addressing a single ion with tightly focused laser beams is required during the cooling and fluorescence detection stages to prevent the light manipulating the auxiliary ion from destroying the coherence in the target ion. Alternatively, a third ion of a different species can be used for sympathetic cooling purposes.

Let us denote Pauli operators acting on the target state by $\hat{\sigma}_j$, and Pauli operators acting on the auxiliary atom by $\overline{\sigma}_j$, for $j = x,y,z$. Then, after cooling and optical pumping of the auxiliary ion into the upper qubit level, step 3 of the scheme can be represented by the following time-evolution operator:

$$\hat{U} = e^{i\frac{\pi}{4}\overline{\sigma}_y} e^{i\chi\hat{\sigma}_z\overline{\sigma}_z} e^{i\frac{\pi}{4}\overline{\sigma}_x}. \tag{16}$$

The single-particle operations on the auxiliary ion can be carried out with a stimulated Raman interaction acting only on that ion. It is easy to show that choosing $\chi \ll 1$ leads to a final state

$$\begin{aligned} |\psi_f\rangle = e^{i\frac{\pi}{4}}\{&[ic_1(1+\chi)|g\rangle + ic_2(1-\chi)|e\rangle]|\downarrow\rangle \\ &+ [c_1(1-\chi)|g\rangle + c_2(1+\chi)|e\rangle]|\uparrow\rangle\}. \end{aligned} \tag{17}$$

Now making a projective measurement of the auxiliary atom spin state, step 4, realizes the unsharp measurement on the target state, similarly to the final step in scheme I. Note that the effect of the squeezing operator $\chi\hat{\sigma}_z\overline{\sigma}_z$ is equivalent to that of the Kitegawa operator $(\chi/2)\hat{J}_z^2$ up to a global phase factor that can be neglected.

IV. UNSHARP MEASUREMENT FIDELITY

Each of the schemes presented above is subject to experimental imperfections. We now take stock of the most important sources of errors that would deteriorate the efficacy with which each unsharp measurement can be executed. In what follows we assume throughout that the laser light interacting with the ion has 5 mW of power focused to a spot size with a diameter of 50 μm, a conservative estimate for the light intensities achievable in a typical laboratory at UV wavelengths.

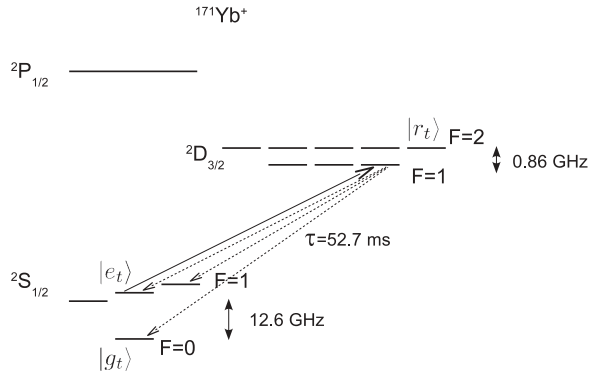

FIG. 4. Energy levels of an $^{171}Yb^+$ ion. The hyperfine ground states $|^2S_{\frac{1}{2}}, F = 0, m_F = 0\rangle$ and $|^2S_{\frac{1}{2}}, F = 1, m_F = 0\rangle$ (clock states) serve as qubit levels undergoing Rabi oscillations. The metastable state $|^2D_{\frac{3}{2}}, F = 1, m_F = +1\rangle$ assists in implementing the unsharp measurement. The dashed arrows show possible spontaneous decay paths. Raman scattering to the $|^2S_{\frac{1}{2}}, F = 1, m_F = +1\rangle$ state removes the ion from the oscillating qubit transition and halts the experiment.

A. Scheme I fidelity

For concreteness we take $^{171}Yb^+$ as a candidate for the target atom in the scheme I implementation. The clock transition, $|^2S_{\frac{1}{2}}, F = 0, m_F = 0\rangle \longrightarrow |^2S_{\frac{1}{2}}, F = 1, m_F = 0\rangle$, is chosen as a qubit. In addition, a suitable metastable level is needed for implementation of this scheme. The $|^2D_{\frac{3}{2}}, F = 1, m_F = +1\rangle$ with a lifetime of $\tau = 52.7$ ms can serve this purpose. The level scheme for $^{171}Yb^+$ is illustrated in Fig. 4.

1. Spontaneous emission

While the $^2D_{3/2}$ state, $|r_t\rangle$, in ytterbium is metastable (electric quadrupole transition), its $\tau_{sp} = 52.7$ ms lifetime does not make the scheme completely immune to spontaneous emission. To find an upper bound to the effect of spontaneous emission we calculate the emission rate if an ion would spend the entire time it takes to implement the four preparation pulses in $|r_t\rangle$. The time δt to implement the four pulses is roughly set by the RSB pulse rather than the carrier pulse, since for the RSB pulse the coupling with the laser field is reduced by a factor corresponding to the Lamb-Dicke parameter, η_{LD} [18], as compared to the carrier pulse. The lifetime of the metastable state allows us to estimate the quadrupole matrix element from

$$\mu_q = \sqrt{\frac{3\pi c\epsilon_0\gamma_q}{\omega^3}}, \tag{18}$$

where $\gamma_q = 1/\tau_{sp}$, c is the speed of light, ϵ_0 the permittivity of free space, and ω_q the angular frequency of the transition. For our typical laser parameters (5 mW and a focus spot width of diameter 50 μm), we find an electric field strength estimate of $E_0 = \sqrt{2I/(c\epsilon_0)} \approx 22$ kV/m. This predicts a RSB pulse coupling frequency of $\Omega_{\mathrm{RSB}} = 2\pi/\tau_{\mathrm{RSB}} = \eta_{\mathrm{LD}}\mu_q E_0/(4\hbar) \approx 2\pi \times (70$ kHz). The probability that the ion did *not* spontaneously emit from the level $|r_t\rangle$ at the end of $\delta t \approx 2\tau_{\mathrm{RSB}} \approx 15$ μs is $\exp(-\delta t/\tau_{sp})$. We can therefore calculate the number of excitations to $|r_t\rangle$ which predict a 50% chance of decay as $N = -(\tau_{sp}/\delta t)\ln(0.5) \approx 1100$ or, otherwise stated, the probability for spontaneous scattering per measurement is $P_{sp} = 0.0007$.

It is worth noting that different spontaneous emission channels exist, not all being equally deleterious. The ion might Rayleigh scatter back into the ground state from which it is driven, Raman scatter into the other qubit state, or even Raman scatter out of the qubit transition. A Raman-scattering event to a different qubit state will completely destroy the coherence in the target qubit, and situations can arise in which Rayleigh scattering also becomes strongly decohering [21]. Spontaneous emission problems can be overcome by choosing an ion with a much longer-lived metastable state, or with no spontaneous emission path that would remove the ion from the qubit levels.

2. *Imperfect quantum logic spectroscopy*

The state mapping during QLS is not perfect. Incorrect mapping might, for example, occur because external heating of the ion causes an unintended excitation of the motional mode [22], or due to a spontaneous scattering from the auxiliary ion. During an unsharp measurement sequence this translates to the experimenter measuring a false outcome $\hat{M}_0$ instead of $\hat{M}_1$ or vice versa. Since external factors such as motional heating are very much dependent on the specific ion-trap geometry, of which there are many kinds, we do not attempt to estimate the typical probability of incorrect mapping. Instead we only evaluate experimental fidelities for different applications of unsharp measurements, at different probabilities of incorrect mapping, in later sections.

B. Scheme II fidelity

Measurement fidelity in our second scheme is also limited by the effects of spontaneous emission. The detection scheme, however, does not rely on QLS and the concomitant state mapping errors are absent.

1. *Spontaneous emission from optical dipole fields*

Whereas in scheme I we were concerned with decoherence due to spontaneous emission by an atom occupying a metastable excited state, in scheme II we consider the spontaneous scattering of far *off-resonant* light fields. This is a well-studied problem [21,23] and depends sensitively on the polarizations of the light fields, frequency detunings, and detailed atomic structure. Here we make simple order-of-magnitude estimates following a typical scheme for a squeezing Hamiltonian as used in [20] to implement geometric phase gates. We are interested in finding the time needed to implement weak squeezing using this scheme, and we compare it to the spontaneous emission expected during that time. As in [20] we consider two beryllium ions in a trap with stretch-mode frequency of $\omega_s \approx (2\pi) \times 6$ MHz. This motional mode is excited off-resonantly by two interfering laser beams impinging on the trapped ions. The excitation is executed in such a way that the vibrational wave packet traces out a closed loop in phase space. A phase gate is fully implemented when the geometric phase, ϕ_G, which the ions have accumulated is equal to $\pi/2$ [24]. This phase is related to the optical dipole force, F_0, via

$$\phi_G = \frac{\pi}{2}\left(\frac{F_0 z_0 \tau_g}{\hbar}\right)^2, \tag{19}$$

where $z_0 = \sqrt{\hbar/(2m\omega_s)}$ is the width of the stretch-mode ground state, and m the mass of the ion. The laser beams enter at 90° with respect to each other, forming an interference pattern with an effective wave number $k_{\text{eff}} = 2\pi\sqrt{2}/(313\text{ nm})$. Assuming a realistic Lamb-Dicke parameter of $\eta_{\text{LD}} = k_{\text{eff}} z_0 \approx 0.2$ implies an associated width $z_0 \approx 7$ nm. The laser fields cause an ac-Stark energy shift, E_S, on the atomic transitions, with gradients due to the interference pattern on the order of $\partial E_S/\partial z = \mu^2 E_0^2 k_{\text{eff}}/4\hbar^2\Delta$, where Δ is the detuning of the lasers from the excited state ($^2P_{1/2}$) transition, taken to be 80 GHz. Sticking with typical laser parameters 5 mW and 50-μm focus diameter, the gradient predicts an optical dipole force of $F_0 = \hbar\partial E_S/\partial z \approx 16$ zeptonewton (zepto $= 10^{-21}$). The corresponding time to complete a phase gate is about $\tau_g \approx 3\ \mu$s.

The on-resonance coupling strength to the excited state is $g = \mu E_0/\hbar$, but because the laser beam is far off resonance there exists only a very small probability to occupy the excited state, of order $P_u \approx g^2/\Delta^2 \approx 2 \times 10^{-5}$. During an unsharp measurement only weak squeezing will be implemented, say for a time $\tau_g/5$, which is about $n_{sp} \approx 23$ spontaneous decay lifetimes. The probability for a spontaneous emission event over this entire time is roughly $P_{sp} = 1 - (1 - P_u)^{n_{sp}} \approx 0.0005$.

Given the calculated probability of P_{sp}, about 1400 unsharp measurements can be carried out before the likelihood for no spontaneous emission event has decayed to 50%.

V. APPLICATIONS OF UNSHARP MEASUREMENTS

In many applications of POVM measurements a sequence of successive measurements is required. Having investigated the imperfections in single measurements for each of our proposed schemes, we now look at the cumulative effect of many measurements in specific applications. In particular we discuss (1) the efficacy with which real-time state estimation can be done of a two-level system undergoing Rabi oscillations and (2) the efficiency with which qubit states can be prepared using only POVM measurements following a scheme proposed by [25].

A. State estimation fidelity

In previous work [9] we demonstrated that it is in principle possible to monitor quantum dynamics (Rabi oscillations) by executing a sequence of periodic, unsharp measurements as the quantum system evolves. In the presence of classical noise fields this state estimation is still possible, albeit with reduced fidelity. For this estimation process to be successful the relevant time scales in the experiment must obey the inequality condition

$$\tau_{\text{meas}} \ll \tau_R \ll \tau_m \ll \tau_N. \tag{20}$$

Here τ_{meas} is the duration of a single unsharp measurement, τ_R is the Rabi frequency, and τ_N is the decoherence time due to the external noise processes. τ_m is the expected time it takes an arbitrary initial state to reduce to an eigenstate of the measured observable in the absence of dynamics other than measurement [26].

We now calculate the dependence of estimation fidelity on a number of noise sources and operational errors. These include (1) classical dephasing noise resulting from magnetic field fluctuations, fluctuating Stark shifts, and reference oscillator noise; (2) imperfect state mapping during QLS; and (3) spontaneous emission. We now discuss each noise source in turn.

1. Classical dephasing noise

Let us establish whether experimental parameters which will allow us to fulfill condition (20) are realizable. Classical dephasing noise can be described by a Hamiltonian $H = \beta(t)\hat{\sigma}_z$. One convenient measure of the strength of the noise is the ratio of the root-mean-square noise strength, $\Delta\beta$, to the Rabi frequency. This ratio can be determined if the Ramsey coherence time of the qubit states is known. The clock transition is insensitive to magnetic field fluctuations leading to long coherence times. In ytterbium this transition has been reported to have a Ramsey coherence time of 2.5 s [27]. The Ramsey coherence is related to the noise field strength through the noise power spectrum via the expression [28]

$$s(t) = e^{-\frac{8}{\pi}\int_0^\infty \frac{P(\omega)}{\omega^2}\sin^2(\omega t/2)d\omega} \tag{21a}$$

$$\approx e^{-\frac{2}{\pi}\int_0^\infty P(\omega)d\omega t^2}, \tag{21b}$$

where $s(t)$ is the coherence, $P(\omega)$ is the power spectrum of the noise field $\beta(t)$, and the last line follows when $\tau \ll 1$. We further know that $\Delta\beta^2 = \frac{1}{\pi}\int_0^\infty P(\omega)d\omega$, which by comparing to Eq. (21b) allows us to relate the Ramsey coherence time to the mean field strength as $\tau_{\text{Ramsey}} = \tau_N = 1/(\sqrt{2}\Delta\beta)$. Experimentally achievable Rabi oscillation time can be much shorter than τ_{Ramsey}, e.g., around 12 μs reported in [27]. However, to fulfill condition (20) one can experimentally choose $\tau_R \approx 100$ ms. Then with $\tau_{\text{Ramsey}} = 2.5$ s one finds $\Omega_R/\sqrt{2}\Delta\beta = \tau_N/\tau_R \approx 200$. Given perfect, instantaneous unsharp measurements, numerical simulations have shown that this will predict estimation fidelities in excess of $F = 0.999$ [9]. However, several further imperfections need to be considered. We also note that oscillator noise can at any time be introduced artificially into the system to enable testing of the system.

2. Imperfect State Mapping

As discussed earlier, imperfect state mapping during QLS measurements will be strongly affected by trap heating rates which depend on the trap geometry. Rather than try to estimate the typical effect, we therefore demonstrate what the effect on estimation fidelity is as a function of different probabilities for an incorrect mapping. This is plotted in Fig. 5, where we simulated a qubit undergoing Rabi oscillations in the absence of dephasing noise. We used $p_0 = 0.45$ and carried out ten unsharp measurements per oscillation of the z component of the spin. After each measurement we update our state estimate according to Eq. (2) with the correct, or incorrect, measurement operator with probability $1 - P_w$ or P_w, respectively. As seen in Fig. 5 imperfect mapping at the level of about 10% can be tolerated at estimation fidelities around 90%.

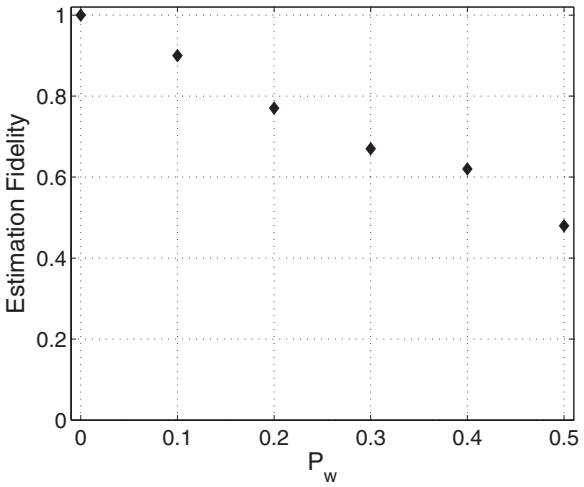

FIG. 5. State estimation fidelity as a function of the probability, P_w, to make a wrong mapping during a QLS measurement.

3. Spontaneous Emission

In Secs. IV A1 and IV B we estimated that spontaneous scattering rates in typical experiments lead to a probability of $P_{sp} \approx 0.0005$–0.001 for a spontaneous scattering event per unsharp measurement. We again characterize the estimation fidelity in a simulation of a two-level system undergoing Rabi oscillations, carrying out ten unsharp measurements per oscillation of the z component of the spin, and using $p_0 = 0.45$. During each measurement we assume a probability of P_{sp} for the qubit state to collapse into either the upper or the lower level with equal probability. The results are summarized in Fig. 6. When compared to the results of Fig. 5 we see that a fixed likelihood per measurement for a spontaneous scattering event is significantly more detrimental than the same likelihood for making an incorrect detection. In particular, in this case $P_{sp} \approx 0.001$ yields an estimation fidelity of 90%, while the same fidelity is achieved with $P_w \approx 0.1$.

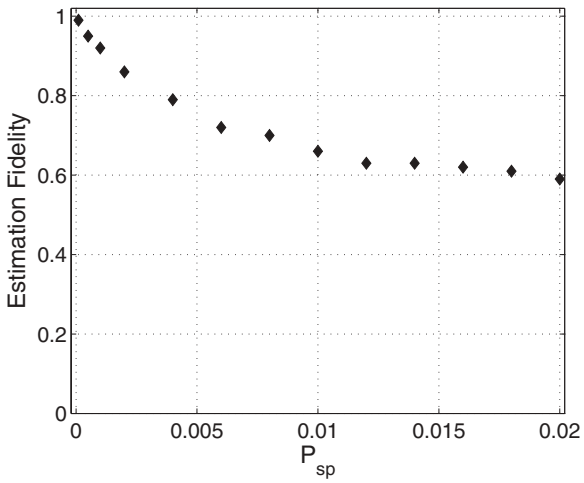

FIG. 6. State estimation fidelity as a function of the probability, P_{sp}, for a spontaneous emission event to take place during an unsharp measurement.

B. State preparation using unsharp measurement

As a second application we consider the state preparation scheme proposed by Ashhab and Nori [25]. They demonstrated that it is possible to prepare arbitrary qubit states using unsharp measurements along only a restricted set of orthogonal axes. For preparing a state

$$|\psi\rangle = \sin\frac{\theta_T}{2}e^{+i\phi_T/2}|0\rangle + \cos\frac{\theta_T}{2}e^{-i\phi_T/2}|1\rangle, \qquad (22)$$

and assuming the state is initially in $|\psi_0\rangle = (|0\rangle + |1\rangle)/\sqrt{2}$, they take the following approach:

(1) Make a sequence of POVM measurements of $\hat{\sigma}_y$ until the qubit phase angle converges to ϕ_T.

(2) Make a sequence of POVM measurements of $\hat{\sigma}_z$ until the polar angle converges to θ_T.

During each of these two steps there is a roughly 50% chance that the qubit wanders in the wrong angular direction. If this happens simply reset the qubit to the state $|\psi_0\rangle$ by making alternately strong, *projective* measurements of $\hat{\sigma}_x$ and $\hat{\sigma}_y$ until the qubit ends up in $|\psi_0\rangle$.

We simulate this procedure in order to prepare the qubit state with angles $\theta_T = \pi/4$ and $\phi_T = \pi/2$. Choosing $p_0 = 0.15$ gives us fast convergence to the target state with a fidelity of $F = |\langle\psi_0|\psi_T\rangle|^2 = 0.998$ within an average of 22 measurements. Again we test the performance of the preparation scheme when spontaneous emission or imperfect state mapping is present during the unsharp measurements. Figure 7(a) shows the decay of the state preparation fidelity as a function of the probability per measurement, P_{sp}, for a spontaneous emission event to take place. The corresponding average number of measurements to convergence is shown in Fig. 7(b), demonstrating that it requires more measurements to converge in the presence of stronger spontaneous scattering. In Figs. 8(a) and 8(b) similar curves are plotted for different likelihoods of imperfect state mapping. We see that state preparation at fidelities above 90% should be possible if the likelihood of spontaneous emission and incorrect detection can be maintained below 10% per measurement.

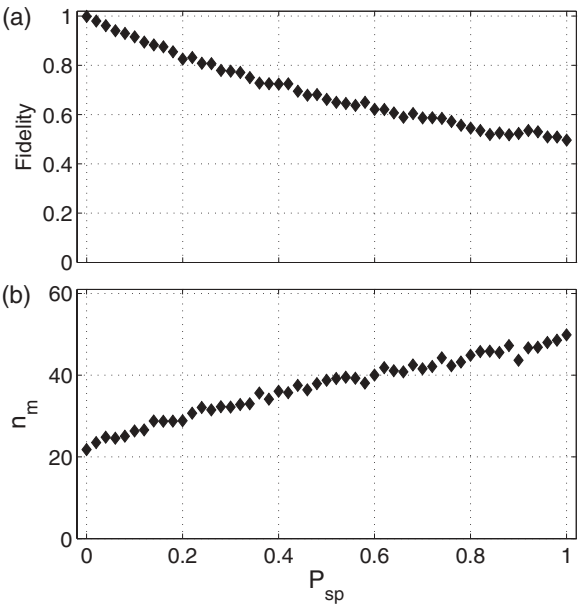

FIG. 7. Performance of POVM measurement state preparation scheme in the presence of spontaneous emission. (a) State preparation fidelity as a function of the probability per measurement for a spontaneous emission event to take place. (b) Number of measurements to convergence as a function of the probability per measurement for a spontaneous emission event to take place.

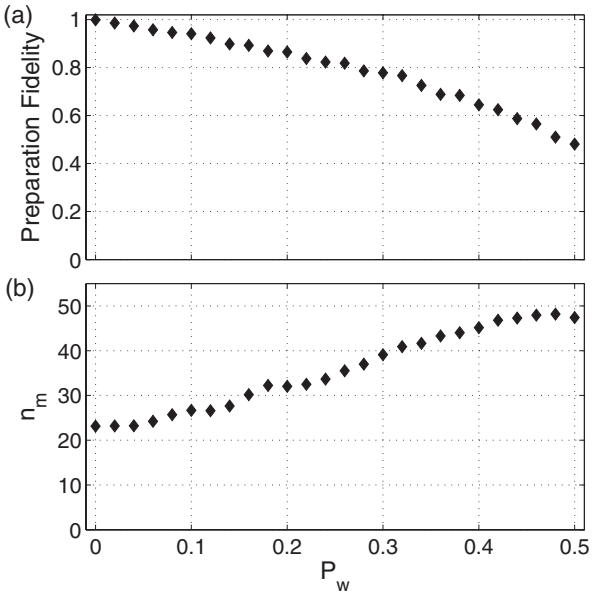

FIG. 8. Performance of POVM measurement state preparation scheme in the presence of imperfect detection of the auxiliary ion state. (a) State preparation fidelity as a function of the probability per measurement for an incorrect detection to take place. (b) Number of measurements to convergence as a function of the probability per measurement for an incorrect detection to take place.

VI. CONCLUSION

In conclusion, we have shown here how to realize a class of symmetric POVM measurements on the qubit levels of a trapped ion. Having analyzed the most common sources of error these measurements will be subject to, we conclude that convincing proof-of-principle experiments of applications of unsharp measurements should be possible by exploiting standard ion-trap quantum control techniques. This work expands the set of tools available to ion-trap quantum control experimentalists and opens the door to exploring new applications such as real-time quantum state monitoring or quantum feedback using unsharp measurements.

APPENDIX: PREPARATION OF AN ARBITRARY SYMMETRIC POVM

We discuss how to implement a POVM measurement of the form defined by Eqs. (1), (3), and (4) for arbitrary $\hat{r} = \sin\theta\cos\phi\ \hat{x} + \sin\theta\sin\phi\ \hat{y} + \cos\theta\ \hat{z}$. We only present an approach based on scheme I. Explicitly the two measurement

operators are

$$\hat{M}_0 = \frac{1}{2}\begin{pmatrix} p_+ + p_- \cos\theta & p_- \sin\theta e^{-i\phi} \\ p_- \sin\theta e^{+i\phi} & p_+ - p_- \cos\theta \end{pmatrix}, \quad \text{(A1)}$$

and

$$\hat{M}_1 = \frac{1}{2}\begin{pmatrix} p_+ - p_- \cos\theta & -p_- \sin\theta e^{-i\phi} \\ -p_- \sin\theta e^{+i\phi} & p_+ + p_- \cos\theta \end{pmatrix}, \quad \text{(A2)}$$

where $p_\pm = \sqrt{p_0} \pm \sqrt{1-p_0}$. If the target and auxiliary state is initially

$$|\psi_0\rangle = (c_1|g\rangle + c_2|e\rangle)\,|1\rangle, \quad \text{(A3)}$$

then to realize the measurement operators Eqs. (A1) and (A2), we must prepare the state

$$|\psi_0\rangle = \left[\frac{c_1}{2}[p_+ - p_-(\cos\theta - \sin\theta e^{-i\phi})]|g\rangle + \frac{c_2}{2}[p_+ + p_-(\cos\theta + \sin\theta e^{+i\phi})]|e\rangle\right]|0\rangle$$

$$+ \left[\frac{c_1}{2}[p_+ + p_-(\cos\theta - \sin\theta e^{-i\phi})]|g\rangle + \frac{c_2}{2}[p_+ - p_-(\cos\theta + \sin\theta e^{+i\phi})]|e\rangle\right]|1\rangle. \quad \text{(A4)}$$

A projective measurement on the auxiliary state will then affect the POVM measurement on the target state. To simplify our discussion we regroup the kets in Eq. (A4) and write each coefficient as a single complex number:

$$|\psi\rangle = c_1\,(a_1|0\rangle + a_2|1\rangle)\,|g\rangle + c_2\,(b_1|0\rangle + b_2|1\rangle)\,|e\rangle. \quad \text{(A5)}$$

Once the direction, $\hat{r}$, and the strength, p_0, of the POVM measurement have been chosen, the coefficients in Eq. (A5) can be found by direct comparison with Eq. (A4). The desired state is prepared by simply doing single-qubit rotations on the transition $|g_t\rangle \rightarrow |r_t\rangle$ to have the same coefficients a_1 and a_2, as in Eq. (A5), during the first carrier pulse of the four-pulse measurement preparation sequence. The RSB pulse then maps the auxiliary states to give the term multiplying $|g_t\rangle$ in Eq. (A5). The procedure is then repeated on the $|e_t\rangle \rightarrow |r_t\rangle$ transition.

[1] D. Wineland, M. Barret, J. Britton, J. Chiaverini, B. DeMarco, W. Itano, B. Jelenkovic, C. Langer, D. Leibfried, V. Meyer, T. Rosenband, and T. Schätz, Philos. Trans. R. Soc. Lond. A **361**, 1349 (2003).

[2] P. Schmidt, T. Rosenband, C. Langer, W. Itano, J. Bergquist, and D. Wineland, Science **309**, 2005 (2005).

[3] G. Hetet, L. Slodicka, M. Hennrich, and R. Blatt, Phys. Rev. Lett. **107**, 133002 (2011).

[4] R. Blatt and C. Roos, Nat. Phys. **8**, 277 (2012).

[5] M. A. Nielsen and I. Chuang, *Quantum Computation and Quantum Information* (Cambridge University Press, Cambridge, UK, 2002).

[6] N. Katz, M. Ansmann, R. Bialczak, E. Lucero, R. McDermott, M. Neeley, M. Steffen, E. Weig, A. Cleland, J. Martinis, and A. N. Korotkov, Science **312**, 1498 (2006).

[7] C. Sayrin, I. Dotsenko, X. Zhou, B. Peaudecerf, T. Rybarczyk, S. Gleyzes, P. Rouchon, M. Mirrahimi, H. Amini, M. Brune, J.-M. Raimond, and S. Haroche, Nature (London) **477**, 73 (2011).

[8] G. G. Gillett, R. B. Dalton, B. P. Lanyon, M. P. Almeida, M. Barbieri, G. J. Pryde, J. L. O'Brien, K. J. Resch, S. D. Bartlett, and A. G. White, Phys. Rev. Lett. **104**, 080503 (2010).

[9] T. Konrad and H. Uys, Phys. Rev. A **85**, 012102 (2012).

[10] J. Audretsch, F. Klee, and T. Konrad, Phys. Lett. A **361**, 212 (2007).

[11] J. F. Ralph, K. Jacobs, and C. D. Hill, Phys. Rev. A **84**, 052119 (2011).

[12] R. Vijay, C. Macklin, D. Slichter, S. Weber, K. Murch, R. Naik, A. Korotkov, and I. Siddiqi, Nature (London) **490**, 77 (2012).

[13] R. Ruskov and A. N. Korotkov, Phys. Rev. B **66**, 041401(R) (2002).

[14] A. N. Jordan and A. N. Korotkov, Phys. Rev. B **74**, 085307 (2006).

[15] Y.-S. Kim, Y.-W. Cho, Y.-S. Ra, and Y.-H. Kim, Opt. Exp. **17**, 11978 (2009).

[16] A. N. Korotkov and A. N. Jordan, Phys. Rev. Lett. **97**, 166805 (2006).

[17] J. Audretsch, T. Konrad, and A. Scherer, Phys. Rev. A **65**, 033814 (2002).

[18] D. Wineland, C. Monroe, W. Itano, D. Leibfried, B. King, and D. Meekhof, J. Res. Natl. Inst. Stand. Technol. **103**, 259 (1998).

[19] M. Kitagawa and M. Ueda, Phys. Rev. A **47**, 5138 (1993).

[20] D. Leibfried, B. DeMarco, V. Meyer, D. Lucas, M. Barret, J. Britton, W. Itano, B. Jelenkovic, C. Langer, T. Rosenband, and D. J. Wineland, Nature (London) **422**, 412 (2003).

[21] H. Uys, M. J. Biercuk, A. P. VanDevender, C. Ospelkaus, D. Meiser, R. Ozeri, and J. J. Bollinger, Phys. Rev. Lett. **105**, 200401 (2010).

[22] L. Deslauriers, S. Olmschenk, D. Stick, W. K. Hensinger, J. Sterk, and C. Monroe, Phys. Rev. Lett. **97**, 103007 (2006).

[23] R. Ozeri, C. Langer, J. Jost, B. DeMarco, A. Ben-Kish, B. Blakestad, J. Britton, J. Chiaverini, W. Itano, D. Hume, D. Leibfried, T. Rosenband, P. O. Schmidt, and D. J. Wineland, Phys. Rev. Lett. **95**, 030403 (2005).

[24] R. Ozeri, Contemp. Phys. **52**, 531 (2011).

[25] S. Ashhab and F. Nori, Phys. Rev. A **82**, 062103 (2010).

[26] J. Audretsch, L. Diósi, and T. Konrad, Phys. Rev. A **66**, 022310 (2002).

[27] S. Olmschenk, K. C. Younge, D. L. Moehring, D. Matsukevich, P. Maunz, and C. Monroe, Phys. Rev. A **76**, 052314 (2007).

[28] G. Uhrig, New. J. Phys. **10**, 083024 (2008).